Journal of Materials Chemistry C

Accepted Manuscript

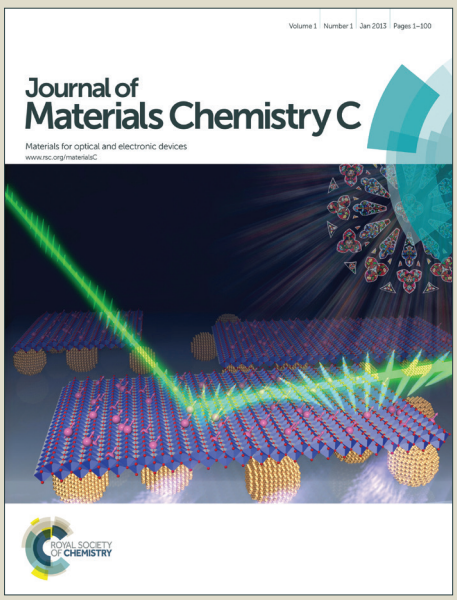

ROYAL SOCIETY OF CHEMISTRY

www.rsc.org/materialsC

Journal Name

RSCPublishing

ARTICLE

Heteroatom induced contrasting effects on the stimuli responsive properties of anthracene based donor-π-acceptor fluorophores

Cite this: DOI: 10.1039/x0xx00000x

Received 00th January 2012,
Accepted 00th January 2012

DOI: 10.1039/x0xx00000x

www.rsc.org/

Karattu Chali Naeem,[a,b] Akhila Subhakumari,[a] Sunil Varughese[c] and Vijayakumar C. Nair*[a,b]

Two donor-π-acceptor type fluorophores consisting of anthracene as the donor and benzoxazole (**ABO**) or benzothiazole (**ABT**) as the acceptor are synthesised. Both fluorophores exhibit excellent solid state luminescence, and respond to external stimuli such as mechanical force (mechanochromism) and protons (acidochromism). Though the differences between the two molecules are marginal, their stimuli responsive behaviours are contrasting. **ABO** shows stable mechanochromism but the protonation induced colour change is unstable. On the other hand, **ABT** shows stable acidochromism but luminescence changes induced by mechanical stress reverted back quickly. Detailed study reveals that the variance in the heteroatoms in benzoxazole/benzothiazole moieties (oxygen and sulphur, respectively) significantly affect both the intra- and intermolecular electronic interactions of the molecules resulting in such observations. In the case of **ABO**, the benzoxazole moieties interacts through weak edge-to-edge π-stacking, whereas in **ABT**, the ring overlap is more significant making the π-stacking a stronger face-to-face type, which helps the restoration of the molecular ordering in **ABT** energetically more viable. Regarding the acidochromic properties, the presence of more electronegative oxygen (compared to sulphur) in **ABO** draws electrons efficiently towards it making the nitrogen less basic and the complex formed between **ABO** and TFA less stable. On the other hand, electron density on the nitrogen in **ABT** might be higher compared to **ABO** due to the presence of less electronegative sulphur leading to the formation of a stable complex between **ABT** and TFA.

Introduction

Organic smart materials exhibiting dynamic and reversible switching of fluorescence attract growing attention from material scientists.[1] Several organic molecules showing switchable solid state luminescence on exposure to external stimuli such as light, heat, chemical, electrical, and mechanical have been reported during the last decade.[2] Among them, mechanochromic luminescent materials are particularly important because of their fundamental relevance and potential for applications in sensors, optical information storage, memory devices, and security inks.[3] However, studies on such materials remain in the relatively nascent stages when compared to that of other classes of stimuli responsive materials. Mechanochromic luminescence responses are in general can be induced in supramolecular assemblies through the changes in intermolecular interactions such as π-π stacking and hydrogen bonding existing between molecules.[4] Presence of such supra-molecular forces fixes the orientation and packing of the fluorophore in a definite manner in the (self-assembled) solid-state. On mechanical perturbation, these weak forces break, and the chromophores undergo disorientation resulting in the switching of the colour and luminescence properties.

Contrary to mechanochromism, acidochromism can be induced by the modulation of the intramolecular electronic delocalization in a molecular system.[5] Molecules containing nitrogen, for instance, found to be responsive to acids because of the easy availability of the lone pair on nitrogen for proton binding.[6] If the nitrogen atom is placed in conjugation with the chromophore, protonation on the nitrogen may change the electron distribution and hence the colour and luminescence of the molecules. Studies have proved that control over the stimuli responsive behaviours of molecules and materials could be achieved through the control of inter- and intramolecular interactions *via* rational designing. Towards this end, a precise knowledge on the structure-property relationship and a deeper understanding of the mechanisms responsible for the stimuli responsive properties of the molecules are required.

In the present work, we try to understand how small variations on the basic chromophore structure affect the intermolecular and intramolecular interactions of anthracene based chromophores and their stimuli responsive behaviours, particularly mechanochromism and acidochromism. Though anthracene is a well-studied fluorophore, anthracene based mechano-responsive systems are reported recently only. Most of the reports consist of distyryl substituted anthracene conjugated to various chromophores such as tetra-phenylethylene, triphenylethylene, carbazole, phenothiazine, pyridine, fluorene and *N*-alkyl benzene.[7] Some of these fluorophores exhibit both mechanochromism and acido-chromism.[8] Various groups have studied the effect of the nature and number of end groups and alkyl chain lengths on the stimuli responsive behaviours of anthracene derivatives.[9]

Herein, we have synthesized two donor-π-acceptor type fluorophores consisting of anthracene as the donor and benzoxazole (**ABO**) or benzothiazole (**ABT**)[10] as the acceptor (Scheme 1). Both benzoxazole and benzothiazole acceptors contain two heteroatoms; nitrogen is present in both, whereas,

oxygen present in the former and sulphur in the latter. It should be noted that both oxygen and sulphur belongs to same group and have comparable electronic structures. However, our studies revealed that their influence on the mechano- and acid-responsive properties of **ABO** and **ABT** was contrasting in nature.

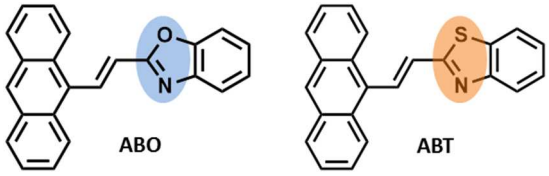

Scheme 1. Chemical structure of the anthracene-benzoxazole (**ABO**) and anthracene-benzothiazole (**ABT**) derivatives under study.

Experimental

Materials

The reagents and materials for synthesis were purchased either from local suppliers or from Sigma-Aldrich or Alfa Aeser and used as received. Air and water sensitive synthetic steps were performed in an argon atmosphere using standard Schlenk techniques.

Measurements

Melting points were determined with a Mel-Temp-II melting point apparatus and are uncorrected. ^{1}H and ^{13}C-NMR spectra were recorded on a 500 MHz Bruker Avance II spectrometer. All the chemical shifts were referenced to $(CH_3)_4Si$ (TMS; δ = 0 ppm) for ^{1}H or residual $CHCl_3$ (δ = 77 ppm) for ^{13}C. High resolution mass spectral (HRMS) analysis was obtained from a JEOL JM AX 505 HA instrument.

Differential scanning calorimetry (DSC): Differential scanning calorimetric experiments were performed using a Perkin-Elmer Pyris 6 DSC instrument in sealed aluminium pans under nitrogen flow, at heat/cooling rate of 10 °C/min.

Thermal gravimetric analysis (TGA): Thermal gravimetric analysis of the samples was carried out using Schimadzu DTG-60 TG analyser. The samples were heated from room temperature to 600 °C at a heating rate of 10 °C/ min in N_2 atmosphere.

Absorption and fluorescence spectroscopy: Absorption spectra were recorded using Shimadzu UV-Visible-3101 PC NIR scanning spectrophotometer using quarts cuvette with 1 cm path length. Fluorescence spectra were collected using SPEX-Fluorolog F112X Spectrofluorimeter equipped with a 450 W Xenon arc lamp. The obtained spectra were corrected using the program supplied by the manufacturer.

Fluorescence quantum yield and lifetime: The quantum yields of fluorescence in solution were calculated relative to standard compounds (Quinine sulphate in 0.1 M H_2SO_4; ϕ_F = 0.546) using optically matching solutions. Fluorescence lifetimes were measured using an IBH (FluoroCube) time correlated picosecond single photon counting (TCSPC) system. Samples were excited using a pulsed diode laser (< 100 ps pulse duration) at a wavelength of 375 nm (NanoLED-11) with a repetition rate of 1 MHz.

Solid state quantum yield: Photoluminescence quantum yield of the powder samples were measured using a calibrated integrating sphere in a SPEX Fluorolog Spectrofluorimeter. Samples were excited at 365 nm using a Xe-arc lamp as the excitation source. Absolute quantum yield was calculated on the basis of the de Mello method.[11]

Powder XRD measurements: Powder X-ray diffraction (PXRD) patterns of the samples were recorded using the Cu K_α radiation (1.542A˚) on a Philips X'pert PROX-Ray Diffractometer.

Single crystal XRD: Single crystals suitable for X-ray diffraction studies were carefully chosen after they were viewed through a microscope supported by a rotating polarizing stage and a CCD camera. The diffraction data of single crystals were collected on a Rigaku Saturn 724+ diffractometer using graphite monochromated Mo-K_α radiation, and the data was processed with the Rigaku CrystalClear software.[12] The structure solution was carried out by direct methods, and the refinements were performed by full-matrix least-squares on F^2 using the SHELXTL[13] suite of programs. All calculations of intermolecular interactions were done with the HBOND NORM option of PLATON.[14]

Synthesis and Characterization

*Synthesis of **ABO***: 2-methylbenzoxazole (322 mg, 2.42 mmol, 1 equiv.) in dry THF (5 mL) was added to a suspension of *t*-BuOK (543 mg, 4.84 mmol, 2 equiv.) in dry THF (8 mL) kept at 0 °C, and stirred for 1 hour. To this solution, 9-anthracenealdehyde (500 mg, 2.42 mmol, 1equiv.) in dry THF (5 mL) was added drop wise and continued stirring for 1 hour at 0 °C. The reaction mixture was then poured into water and extracted with CH_2Cl_2. The organic extracts were washed with brine and dried over anhydrous Na_2SO_4. The solvent was removed under reduced pressure and the mixture was purified by column chromatography (silica gel, 50% CH_2Cl_2-hexane. The product was recrystallized from CH_2Cl_2-hexane (2:1) mixture to yield the yellow coloured crystals. Yield: 62%; m.p.: 162 ^{o}C; δ_H (500 MHz, $CDCl_3$): 7.08 (d, J = 16.5 Hz, 1H), 7.39-7.44 (m, 2H), 7.51-7.56 (m, 4H), 7.63 (d, J = 9.0 Hz, 1H), 7.81 (d, J = 8.5 Hz, 1H), 8.05 (d, J = 8.5 Hz, 2H), 8.38 (d, J = 8.0 Hz, 2H), 8.49 (s, 1H), 8.74 (d, J = 16.5 Hz, 1H) ppm; δ_C (125 MHz, $CDCl_3$): 110.54, 120.16, 122.81, 124.71, 125.32, 125.42, 125.54, 126.36, 128.20, 128.92, 129.53, 129.88, 131.37, 136.52, 142.16, 150.16, 162.06 ppm; IR (KBr) ν_{max}: 3050, 3024, 1940, 1903, 1820, 1778, 1647, 1538, 1451, 1348, 1305, 1240, 1179, 1098, 973, 929, 891, 859, 788, 739, 625, 603, 543 cm^{-1}; HRMS-FAB+ *m/z* = 322.76 (calc. = 321.27).

*Synthesis of **ABT***: Procedure described above was followed using 2-methylbenzothiazole (361 mg, 2.42 mmol, 1.0 equiv.), 9-anthracene-aldehyde (500 mg, 2.42 mmol, 1.0 equiv.), *t*-BuOK (597.4 mg, 5.32 mmol, 2.2 equiv.) and dry THF (18 mL). The crude product was purified by column chromatography (silica gel, 70% CH_2Cl_2 - hexane) followed by recrystallization from CH_2Cl_2-hexane (2:1) mixture to yield yellow coloured crystals. Yield: 57%, m.p.: 172 ^{o}C; δ_H (500 MHz, $CDCl_3$): 7.36 (d, J = 16.5 Hz, 1H) 7.43 (t, 1H) 7.51-7.56 (m, 5H) 7.95 (d, J = 7.5 Hz, 1H) 8.05 (d, J = 7.5 Hz, 2H) 8.08 (d, J = 8.0 Hz, 1H) 8.37 (d, J = 9.5 Hz, 2H) 8.45 (d, J = 16 Hz, 1H) 8.47 (s, 1H) ppm; δ_C (125 MHz, $CDCl_3$): 121.65, 123.25, 125.41, 125.42, 125.62, 126.27, 126.49, 128.01, 128.90, 129.58, 130.08, 130.72, 131.40, 134.48, 134.51, 153.94, 166.64 ppm; IR (KBr) ν_{max}: 3045, 2997, 1952, 1908, 1820, 1778, 1631, 1484, 1435, 1315, 1283, 1250, 1201, 1158, 1011, 962, 891, 848, 788, 755, 739, 674, 625, 603, 549, 521 cm^{-1}; HRMS-FAB+ *m/z* = 338.76 (calc. = 337.44)

Results and discussion

Synthesis and characterization

ABO and **ABT** were synthesised by the Knoevenagel condensation reaction between 9-anthracenealdehyde and 2-methylbenzoxazole or 2-methylbenzothiazole, respectively. Both compounds were characterized by various analytical

techniques such as ^{1}H NMR, ^{13}C NMR, IR and high-resolution mass spectrometry. They were soluble in common organic solvents like hexane, toluene, tetrahydrofuran (THF), dimethyl formamide (DMF) etc. Analytical techniques such as differential scanning calorimetry (Figure 1a) and thermal gravimetric analysis (Figure 1b) were carried out for the thermal characterization of the bulk material. Heating cycle in the DSC thermograms of the solid samples exhibited an endothermic transition at 162 °C for **ABO** and 172 °C for **ABT**, which correspond to their respective melting transitions. In the cooling cycle, **ABO** showed an exothermic peak at 131 °C with a shoulder at 126 °C, whereas **ABT** exhibited an exothermic peak at 118 °C with shoulder at 113 °C. These peaks could be correlated to the crystallization of the respective molecules from their melt state. It is known that the melting point of a substance depends on the strength of the intermolecular forces holding the material together. Consequently, it could be assumed that the intermolecular forces present in **ABT** are stronger when compared to that of **ABO** as the former exhibit higher melting point. Thermal stability of **ABO** and **ABT** in the solid state was obtained from TGA profile. The T_5 value, which corresponds to the temperature at which the material loses 5% of its initial weight, is a quantitative measure of the thermal stability. T_5 values of **ABO** and **ABT** was found to be at 307 and 321 °C respectively. This observation is consistent with the DSC analysis indicating that the stronger intermolecular interactions in **ABT** at the molecular level provide better thermal stability to the bulk material.

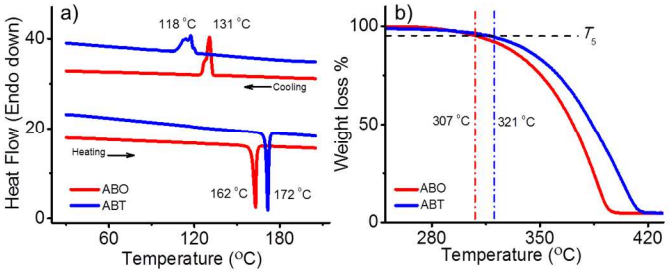

Fig. 1 a) DSC thermograms of **ABO** and **ABT**. b) TGA profiles of **ABO** and **ABT**; the black line indicates the temperatures at which the material loses 5% of its initial weight (T_5).

Photophysical properties in solution state

Table 1. Absorption maximum, emission maximum, extinction coefficient (ε) fluorescence quantum yield (Φ_f) and average fluorescence lifetime of **ABO** and **ABT** in various solvents.

Compound	Solvent	Absorption		Emission		
		λ_{max} (nm)	$\varepsilon \times 10^5$ ($M^{-1}cm^{-1}$)	λ_{max} (nm)	Φ_f (%)[a]	τ (ns)
ABO	Hexane	387	0.12	531	43	3.68
	Toluene	390	0.12	547	18	1.45
	THF	388	0.12	550	3	0.70
	DMF	390	0.12	569	-	-
ABT	Hexane	388	0.10	524	32	2.40
	Toluene	392	0.10	538	6	0.92
	THF	391	0.10	546	1	0.43
	DMF	392	0.10	568	-	-

[a]Quinine sulphate in 0.1 M H_2SO_4 (ϕ_F = 0.546) was used as the standard for quantum yield measurement, error limit ± 5%.

The UV-vis absorption and fluorescence properties of **ABO** and **ABT** were studied in solvents such as hexane, toluene, THF and DMF. The observed photophysical parameters are summarized in Table 1 (conc. = 2 × 10^{-5} M; l = 10 mm; λ_{ex} = 370 nm for fluorescence studies; λ_{ex} = 375 nm for lifetime studies). Absorption characteristics of both molecules were fairly insensitive to the solvent polarity (Figure 2a,b) indicating the molecules are non-polar in the ground state. Both molecules exhibited vibrational features in the absorption spectra in all solvents, which were more pronounced in **ABT**, than that in **ABO**.

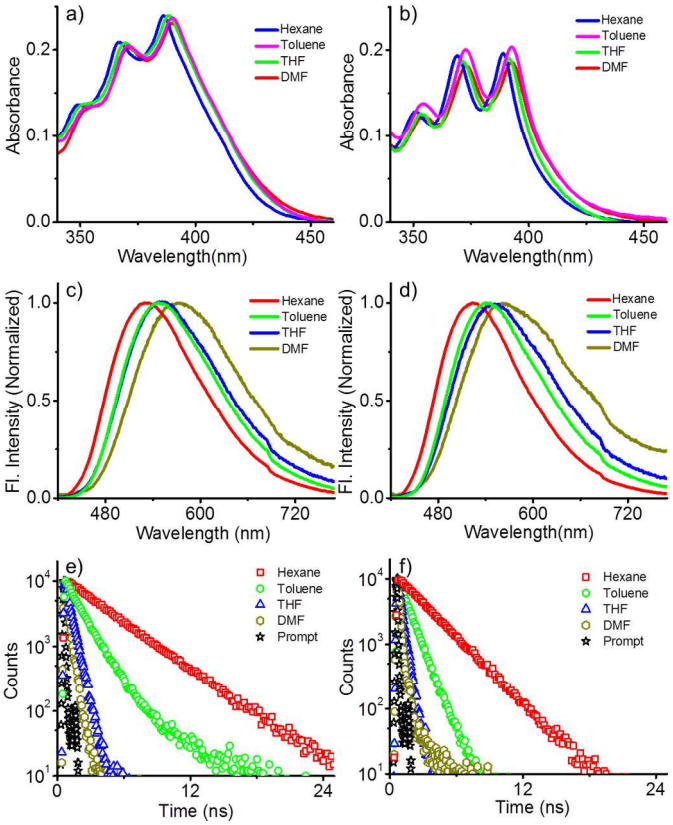

Fig. 2 Absorption spectra of (a) **ABO** and (b) **ABT**; emission spectra of (c) **ABO** and (d) **ABT**; time-resolved fluorescence decay profile of (e) **ABO** and (f) **ABT** recorded in various solvents.

In contrast to the absorption, emission spectra showed red-shift and quenching with increasing solvent polarity (Figure 2c,d) indicating the polar nature of the excited state. Both molecules exhibited maximum luminescence in hexane (least polar solvent among the four) and were non-luminescent in DMF (most polar solvent among the four). The presence of donor and acceptor moieties connected through a π-linker allows the localization of π-electrons towards the acceptor in polar solvents resulting in an internal charge transfer state (ICT) in addition to the locally excited state (LE). ICT state is sensitive to polarity of the environment; energy of which decreases with increase in solvent polarity. Consequently, in polar solvents the energy gap between ground and excited

states will be less, facilitating a faster non-radiative decay to the ground state. This explains the low emission quantum yield and red-shift of the emission maximum in polar solvents.

Excited state lifetime of the molecules in various solvents was calculated from time-correlated single photon counting (TCSPC) analysis (Figure 2e,f). Both compounds exhibited monoexponential decay in hexane, whereas, the decay become biexponential in toluene and THF. In the case of hexane, which is a non-polar solvent, ICT state may not be present, and the emission happens exclusively from the LE state resulting in monoexponential decay. On the other hand, presence of both LE and ICT states results biexponential fluorescence decay in toluene and THF. Fluorescence lifetime of the molecules found to decrease on increasing solvent polarity (Table 1) which is well correlated with the assumptions mentioned above.

Solid state luminescence properties

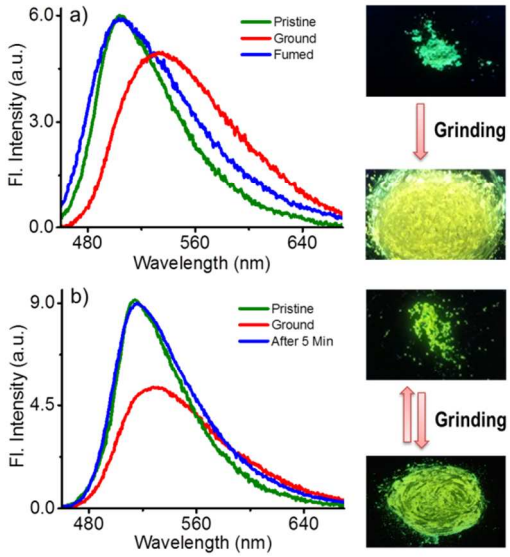

Fig. 3 Photoluminescence spectra of (a) **ABO** and (b) **ABT** under different conditions. Photographs of pristine and ground samples under 365 nm UV irradiation is shown on the right side.

The pristine samples of **ABO** and **ABT** were yellow in colour and emitted green fluorescence on illumination with UV light. The absolute fluorescence quantum yield was 21% for **ABO** and 33% for **ABT**. On mechanical grinding, the green fluorescence of **ABO** changed to yellow. This change in fluorescence was stable and it reversed to the original emission only on solvent (toluene) fuming. **ABT** also showed a similar change in fluorescence as that of **ABO**. However, the fluorescence was unstable; the yellow fluorescence observed on grinding rapidly reverts to the original green emission. The corresponding photo-luminescence spectra are shown in Figure 3. The pristine **ABO** gives emission peak at 504 nm which on grinding, red-shifted to 534 nm, and solvent fuming restores the original emission. In the case of **ABT**, pristine material showed an emission at 514 nm, which changed to 530 nm on grinding. Within 2-3 minutes, the emission spectrum reverted to the original without any external influence. Both molecules exhibited quenching in the emission intensity on mechanical grinding. The fluorescence changes on grinding could be attributed to the destruction of the ordered packing of molecules leading to an amorphous state, and the subsequent changes in the chromophore interactions. This mechanism was confirmed by powder X-ray diffraction (PXRD) analysis Figure S1, ESI†)

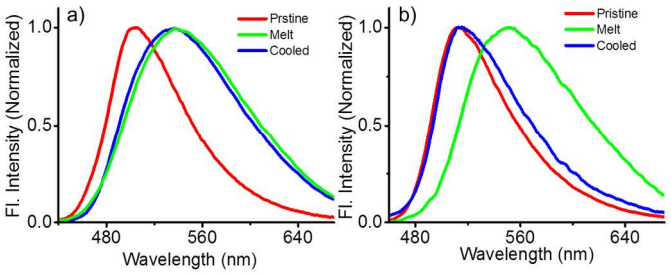

Fig. 4 Emission spectra of pristine, melt and cooled samples of a) **ABO** and b) **ABT** on excitation with 370 nm.

The fluorescence reversal observed in **ABT** was interesting and unprecedented. So we thought it is important to verify the switching behaviour by some other means. As mentioned in the previous section, the fluorescence switching exhibited by both **ABO** and **ABT** on applying mechanical stimuli is due to the transformation of crystalline to amorphous state and the subsequent changes in the chromophore interactions at the molecular level. It was assumed that similar changes can be induced by heating/melting, which also provides a different route to confirm the above observations (however, it must be noted that the melt state and solid amorphous state are different situations). The pristine samples with green emission were heated at 200 ^{o}C for two minutes followed by cooling to room temperature. The emission maximum of **ABO** at 504 nm was red-shifted to 535 nm, which remained there after cooling to room temperature (Figure 4a). On the other hand, the green emission of **ABT** at 514 nm was converted to yellow emission at 548 nm upon heating and it reversed back into the original green emission on cooling (Figure 4b). This study further confirmed the observed luminescence changes of **ABO** and **ABT** obtained on mechanical grinding.

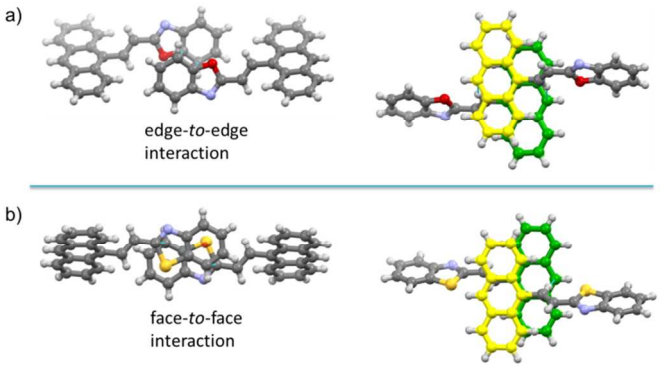

Fig. 5 Interaction between acceptor moieties and donor moieties in (a) **ABO** and (b) **ABT** obtained from single crystal X-ray analysis.

To understand the relationship between mechanochromic stability, supramolecular packing mode and optical properties, single crystals of **ABO** and **ABT** were analysed by using X-ray diffraction measurements (Figure 5). In both cases, the overlapping between the anthracene moieties in their crystal structures were comparable, however, significant differences are observed in the interactions of benzoxazole/benzothiazole moieties. In the case of **ABO**, the benzoxazole moieties make edge-to-edge π-stacking, whereas in **ABT**, the ring overlap is more significant making the π-stacking of

the face-to-face type. The latter interaction being relatively stronger vis-à-vis the former interaction, the restoration of the molecular ordering in the **ABT** is energetically more viable. Thus, the presence of strong non-directional stacking interaction is critical in attaining the reversibility in the mechanochromic behaviour in **ABT**.

Acidochromism

The foregoing section discussed the role of different heteroatoms in the acceptor moiety and the resultant interaction types in yielding variations in the mechanochromic properties. In order to understand how such difference affect the intramolecular interactions, we analyzed the proton sensing ability of these molecules. Upon addition of trifluoroacetic acid (TFA), **ABO** changes color fom yellow to orange forming a new red-shifted shoulder in the absorption spectrum (Figure 6a). On the other hand, **ABT** changes from yellow to red with a new red-shifted, broad absorption band (Figure 6c). Both molecules exhibited emission quenching on the addition of TFA (Figure 6b,d). The quenching was found to be faster in **ABT**. Pronounced change in absorbance and faster quenching of emission suggests that **ABT** interacts more efficiently with TFA than that of **ABO**. This point was further evident from the plot of absorption/emission spectral changes with respect to TFA concentration as shown in Figure 6e and 6f, respectively. The interactions of the compounds with TFA were further confirmed by ^{1}H NMR spectral analysis in the absence and presence of TFA (Figure S2 and S3, ESI †).

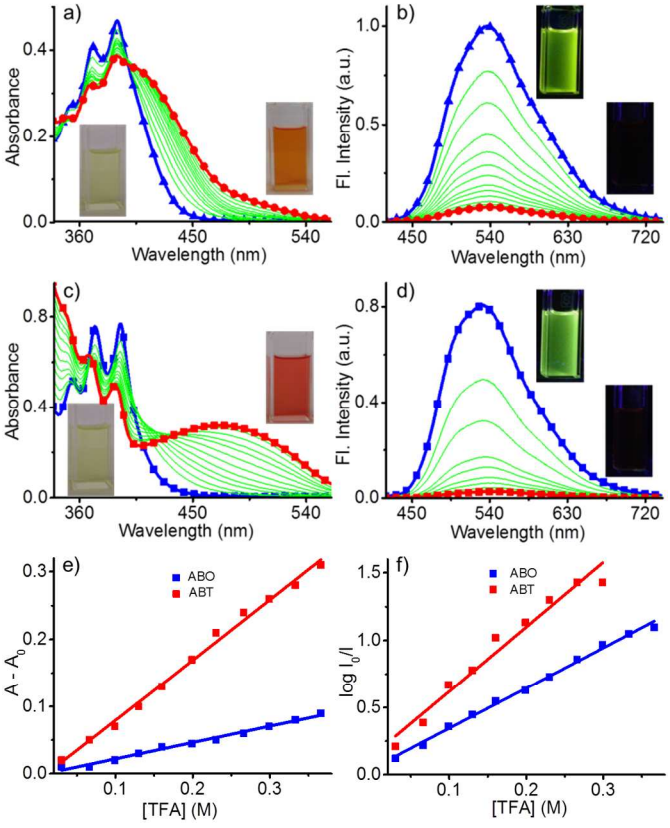

Fig. 6 Absorption changes of a) **ABO** and c) **ABT**; fluorescence changes of b) **ABO** and d) **ABT** on addition of 0 – 60 μL of TFA to the respective solutions in toluene (conc. = 5 × 10^{-5} M, l = 10 mm, λ_{ex} = 370 nm). Photographs of the corresponding solutions are shown in the inset. Plots showing the comparison of the changes in e) absorbance, monitored at 470 nm and f) fluorescence, monitored at 536 nm, of **ABO** and **ABT** with respect to the concentration of TFA.

We explored the acidochromic behaviour of these molecules for making a rewritable media by coating the solutions on a filter paper (Figure 7). In the case of **ABO**, on writing with acid, the letters were clearly visible but it undergone self-erasing within two hours. On the other hand, the letters written on filter paper containing **ABT** were stable, which got erased only on fuming with ammonia. This illustrates that **ABO** can be used as a self-erasable rewritable media and **ABT** can be used as a stable rewritable media. This also implies that the protonated species of **ABT** was stable, whereas that of **ABO** was unstable. This was just contrary to the mechanochromic properties displayed by these molecules, where **ABO** exhibited stable mechanochromism, whereas **ABT** reverted back to the original emission almost instantaneously.

Again the role of heteroatoms could be considered to explain this observation. In both molecules, interaction of TFA must be occurring on nitrogen atom because of the higher basicity of nitrogen compared to that of oxygen/sulphur. The difference in the stability of the complexes formed between TFA and **ABO**/**ABT** could be correlated to the electronegativity difference of oxygen and sulphur relative to nitrogen. The presence of more electronegative oxygen (compared to sulphur) draws electrons efficiently towards it making the nitrogen less basic. As a result, the complex formed between **ABO** and TFA would be less stable resulting in fast dissociation. On the other hand, electron density on the nitrogen in **ABT** might be higher compared to **ABO** due to the presence of less electronegative sulphur leading to the formation of a stable complex.

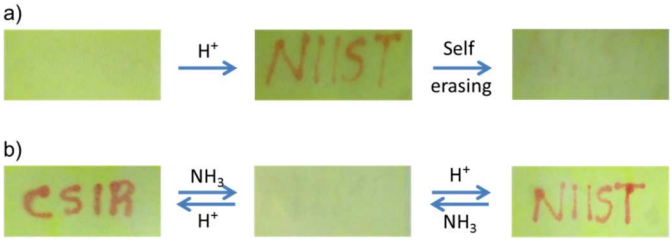

Fig. 7 Photographs of filter papers coated with a) **ABO** and b) **ABT** under different conditions

Though there are several molecules which exhibit multistimuli responsive properties, this is a classic example illustrating how heteroatoms influence the inter- and intramolecular interactions resulting in contrasting stimuli responsive properties. However, the contrast observed on mechanochromic fluorescence switching is less compared to several systems reported in literature.[15] This could be addressed through the rational selection of donor and acceptor moieties, particularly by using a pair of stronger donor and acceptor moieties.

Conclusions

In summary, we have synthesized two multistimuli responsive molecules, which consist of an anthracene (electron donor) connected to benzoxazole (**ABO**)/ benzothiazole (**ABT**) (electron acceptors) through a π-linker. **ABO** showed stable mechanochromic behaviour, whereas, mechanochromic fluorescence changes reverted back instantaneously in the case of **ABT**. The differential interactions between the acceptor moieties arise due to the presence of different heteroatoms were found to be responsible for this observation. More interestingly, the molecules exhibited contrasting

acidochromic properties too. Contrary to the mechanochromism, **ABT** formed stable protonated species, whereas, **ABO** yielded unstable complex with TFA. This difference was also correlated with the difference in the heteroatom present in each molecule. Our study illustrates how small changes in the molecular structure, particularly by incorporating different heteroatoms influence the stimuli responsive properties of organic chromophores. These results may help better design of stimuli responsive materials with precise control over the optical and electronic properties for advanced applications.

Acknowledgements

We thank CSIR network project CSC-0134 (M2D) for financial support. V.C.N. thanks DST for Ramanujan Fellowship (SR/S2/RJN-133/2012). S.V. thanks DST for a young scientist fellowship. K.C.N. is grateful to CSIR for Junior Research Fellowship.

Notes and references

[a] Photosciences and Photonics Section, CSIR-National Institute for Interdisciplinary Science and Technology (NIIST), Trivandrum 695 019, India.

[b] Academy of Scientific and Innovative Research (AcSIR), New Delhi 110 001, India.

c Inorganic and Theoretical Chemistry Section, CSIR-National Institute for Interdisciplinary Science and Technology (NIIST), Trivandrum 695 019, India.

E-mail: cvijayakumar@niist.res.in

† Electronic Supplementary Information (ESI) available: Synthesis scheme, crystal data and structure refinements, PXRD patterns, and ^{1}H NMR spectra. See DOI: 10.1039/b000000x/

1. (a) Z. Chi, X. Zhang, B. Xu, X. Zhou, C. Ma, Y. Zhang, S. Liu and J. Xu, *Chem. Soc. Rev.*, 2012, **41**, 3878–3896.(b) H.-J. Y. and Guey-Sheng, *Chem. Commun.*, 2013, **49**, 9797–9799. (c) X. Wang, O. S. Wolfbeis and R. J. Meier, *Chem. Soc. Rev.*, 2013, **42**, 7834–7869.
2. (a) A. Beneduci, S. Cospito, M. La Deda, L. Veltri and G. Chidichimo, *Nat. Commun.*, 2014, **5**, 3105. (b) W. R. Browne, M. M. Pollard, B. De Lange, A. Meetsma and B. L. Feringa, *J. Am. Chem. Soc.*, 2006, **128**, 12412–12413. (c) A. Seeboth, D. Lotzsch and R. Ruhmann, *J. Mater. Chem. C*, 2013, **1**, 2811–2816. (d) Y. Q. D. and B. zhong T. Xiaoliang Luo, Weijun Zhao, Junqing Shi, Cuihong Li, Zhengping Liu, Zhishan Bo, *J. Phys. Chem. C*, 2012, **116**, 21967–21972. (e) E. Takahashi, H. Takaya and T. Naota, *Chem. - A Eur. J.*, 2010, **16**, 4793–4802.
3. (a) F. Ciardelli, G. Ruggeri and A. Pucci, *Chem. Soc. Rev.*, 2013, **42**, 857–870.(b) Y. Gong, Y. Tan, J. Liu, P. Lu, C. Feng, W. Z. Yuan, Y. Lu, J. Z. Sun, G. He and Y. Zhang, *Chem. Commun.*, 2013, **49**, 4009–4011. (c) S. Yagai, S. Okamura, Y. Nakano, M. Yamauchi, K. Kishikawa, T. Karatsu, A. Kitamura, A. Ueno, D. Kuzuhara, H. Yamada, T. Seki and H. Ito, *Nat. Commun.*, 2014, **5**, 4013.(d) Y. Sagara and T. Kato, *Nat. Chem.*, 2009, **1**, 605–610. (e)X. Zhang, Z. Chi, Y. Zhang, S. Liu and J. Xu, *J. Mater. Chem. C*, 2013, **1**, 3376–3390.
4. (a) S.-J. Yoon and S. Park, *J. Mater. Chem.*, 2011, **21**, 8338–8346. (b) Y. Sagara, T. Mutai, I. Yoshikawa and K. Araki, *J. Am. Chem. Soc.*, 2007, **129**, 1520–1521.(c) S. J. Yoon, J. W. Chung, J. Gierschner, K. S. Kim, M. G. Choi, D. Kim and S. Y. Park, *J. Am. Chem. Soc.*, 2010, **132**, 13675–13683.
5. (a) J. Chen, S. Ma, J. Zhang, L. Wang, L. Ye, B. Li, B. Xu and W. Tian, *J. Phys. chemstry Lett.*, 2014, **5**, 2781–2784. (b) E. L. Spitler, L. D. Shirtcliff and M. M. Haley, *J. Org. Chem.*, 2007, **72**, 86–96. (c) J. Zhang, J. Chen, B. Xu, L. Wang, S. Ma, Y. Dong, B. Li, L. Ye and W. Tian, *Chem. Commun.*, 2013, **49**, 3878–3880.
6. (a) J. Tolosa, K. M. Solntsev, L. M. Tolbert and U. H. F. Bunz, *J. Org. Chem.*, 2010, **75**, 523–534. (b) K. Wang, S. Huang, Y. Zhang, S. Zhao, H. Zhang and Y. Wang, *Chem. Sci.,* 2013, **4**, 3288–3293.
7. (a) Y. Dong, B. Xu, J. Zhang, X. Tan, L. Wang, J. Chen, H. Lv, S. Wen, B. Li, L. Ye, B. Zou and W. Tian, *Angew. Chemie - Int. Ed.*, 2012, **51**, 10782–10785. (b) X. Zhang, Z. Chi, H. Li, B. Xu, X. Li, W. Zhou, S. Liu, Y. Zhang and J. Xu, *Chem. - An Asian J.*, 2011, **6**, 808–811. (c) P. Rajamalli, P. Gandeepan, M.-J. Huang and C.-H. Cheng, *J. Mater. Chem. C*, 2015, **3**, 3329–3335. (d) Y. Dong, J. Zhang, X. Tan, L. Wang, J. Chen, B. Li, L. Ye, B. Xu, B. Zou and W. Tian, *J. Mater. Chem. C*, 2013, **1**, 7554–7559. (e) R. Rao M, C.-W. Liao, W.-L. Su and S.-S. Sun, *J. Mater. Chem. C*, 2013, **1**, 5491–5501. (f) L. Bu, M. Sun, D. Zhang, W. Liu, Y. Wang, M. Zheng, S. Xue and W. Yang, *J. Mater. Chem. C*, 2013, **1**, 2028–2035. (g) Z. Zhang, D. Yao, T. Zhou, H. Zhang and Y. Wang, *Chem. Commun.*, 2011, **47**, 7782–7784. (h) W. Liu, J. Wang, Y. Gao, Q. Sun, S. Xue and W. Yang, *J. Mater. Chem. C*, 2014, **2**, 9028–9034.
8. (a) R. Rao M, C. Liao and S. Sun, *J. Mater. Chem. C*, 2013, **1**, 6386–6394. (b) P. Xue, P. Chen, J. Jia, Q. Xu, J. Sun, B. Yao, Z. Zhang and R. Lu, *Chem. Commun.*, 2014, **50**, 2569–2579.
9. (a) X. Zhang, Z. Chi, B. Xu, C. Chen, X. Zhou, Y. Zhang, S. Liu and J. Xu, *J. Mater. Chem.*, 2012, **22**, 18505–18513. (b) Y. Wang, W. Liu, L. Bu, J. Li, M. Zheng, D. Zhang, M. Sun, Y. Tao, S. Xue and W. Yang, *J. Mater. Chem. C*, 2013, **1**, 856–862. (c) W. Liu, Y. Wang, M. Sun, D. Zhang, M. Zheng and W. Yang, *Chem. Commun.*, 2013, **49**, 6042–6044. (d) L. Bu, M. Sun, D. Zhang, W. Liu, Y. Wang, M. Zheng, S. Xue and W. Yang, *J. Mater. Chem. C*, 2013, **1**, 2028–2035. (e) P. Xue, B. Yao, X. Liu, J. Sun, P. Gong, Z. Zhang, C. Qian, Y. Zhang and R. Lu, *J. Mater. Chem. C*, 2015, **3**, 1018–1025
10. S. E. H. Etaiw, M. K. Awad, T. A. Fayad and M. M. El- hendawy, *J. Mol. Struct*., 2009, **919**, 12-20.
11. J. C. de Mello, H. F. Wittmannn and R. H. Friend, *Adv. Mater.*, 1997, **9**, 230–232.
12. CrystalClear 2.1; Rigaku Corporation: Tokyo, Japan; b) Pflugrath, J. W. *Acta Crystallogr., Sect. D* **1999**, *55*, 1718–1725.
13. Sheldrick, G. M. SHELXTL-PLUS Program for Crystal Structure Solution and Refinement, University of Gottingen, Gottingen, Germany
14. Spek, A. L. PLATON, Molecular Geometry Program, University of Utrecht, The Netherlands, **1995**
15. (a) M. Tanioka, S. Kamino, A. Muranaka, Y. Ooyama, H. Ota, Y. Shirasaki, J. Horigome, M. Ueda, M. Uchiyama, D. Sawada and S. Enomoto, *J. Am. Chem. Soc.*, 2015, **20**, 6436–6439.(b)G. Zhang, J. Sun, P. Xue, Z. Zhang, P. Gong, J. Peng and R. Lu, *J. Mater. Chem. C*, 2015, **3**, 2925–2932.(c) Y. Gong, Y. Tan, J. Liu, P. Lu, C. Feng, W. Z. Yuan, Y. Lu, J. Z. Sun, G. He and Y. Zhang, *Chem. Commun.*, 2013, **49**, 4009–4011 (d) C. Y. K. Chan, J. W. Y. Lam, Z. Zhao, S. Chen, P. Lu, H. H. Y. Sung, H. S. Kwok, Y. Ma, I. D. Williams and B. Z. Tang, *J. Mater. Chem. C*, 2014, **2**, 4320–4327. (e) L. Wang, K. Wang, B. Zou, K. Ye, H. Zhang and Y. Wang, *Adv. Mater.*, 2015, **27**, 2918-2922.

Table of content

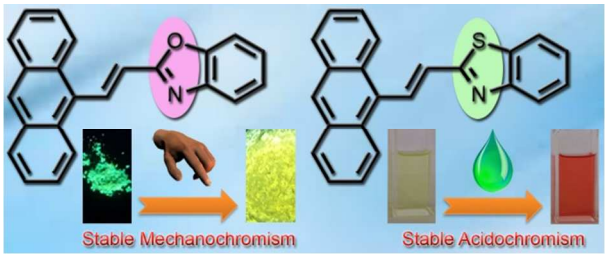

Heteroatom induced differences on mechanochromism and acidochromism of anthracene based fluorophores are described.